Communication

Research on the Thermal Effect of Micro-Channel Cooled Thin-Slab Tm:YAP Lasers

Jianhua Shang [1], Xiaojin Cheng [2,*], Qixin Li [2] and Xiangnan Wu [2]

1   School of Information Science and Technology, Donghua University, Shanghai 201620, China
2   School of Mechanical and Automotive Engineering, Shanghai University of Engineering Science, Shanghai 201620, China
*   Correspondence: xjcheng@sues.edu.cn

Abstract: Using the finite element method and the heat conduction equation, the temperature, stress, and end-face deformation in Tm:YAP crystal under high pump power were analyzed. Combined with gradient doping technology, an effective way to improve the internal heat distribution of the crystal was studied. The results showed that when the total pump power was 200 W, under the same cooling conditions, the maximum temperature difference inside Tm:YAP decreased from 58 K to 25 K after gradient doping. The thermal stress and end-face thermal deformation were also significantly improved. In addition, a reasonable micro-channel structure also effectively removed the heat generated inside the crystal.

Keywords: Tm:YAP; thermal analysis; thin slab; grad-doping

1. Introduction

As a safe band for human eyes, 2-μm lasers have great applications in medical, military, and scientific research, such as coherent Doppler LIDAR, water vapor parabolic surface differential absorption laser radar system, laser remote sensing, laser medical treatment, and as a pump source for 3–5μm lasers [1–3]. Owing to their long fluorescence lifetime and high quantum yield via cross relaxation (about 200%), Thulium tervalent ions are usually doped in YAP, YLF, LLF, and YAG in order to obtain a 2-μm laser [4,5]. With similar thermal and mechanical properties to isotropic YAG, Tm:YAP crystals have received growing attention recently in high-power and high-pulse energy laser output owing to their high emission cross sections for energy storage and their natural birefringence for linearly polarized radiation without the use of extra polarizers [6].

Since the early studies reported by Elder and Payne in 1997, the output power and efficiency of Tm:YAP lasers have increased rapidly [7]. Compared to rod lasers, the slab with a larger aspect ratio (width/thickness) has a better ability for thermal removal, which is mainly adopted in high-power Tm:YAP lasers. In 2017, Jun et al. demonstrated a Tm:YAP double-end-pumped slab laser. The maximum output power of 54.7 W was achieved with a slope efficiency of 44.2% [8]. In 2020, Mao et.al reported a compact dual-end-pumped, 3 at.% a-cut Tm:YAP laser with an output power of 254 W and a slope efficiency of 45.9% [9]. As the pump power increased, the heat dissipation problem became a bottleneck in the Tm:YAP laser. A composite structure was used to improve the thermal distribution inside the Tm:YAP and the thermal distortion at the end face [10]. In 2019, Yuan et al. showed a dual-end-pumped b-cut YAP/Tm:YAP/YAP composite crystal rod laser. The maximum output power of 109.5 W was obtained with an optical-to-optical efficiency of 36.3% [11].

In this paper, a thin-slab Tm:YAP model was constructed and analyzed to present an analytical solution to the heat equation. In addition, by combining the concepts of composite structure, gradient doping, and micro-channel cooling heat sink, the thermal effect of Tm:YAP with different structures was analyzed and compared.

2. Numerical Model

The model of the laser diode- (LD) pumped Tm:YAP crystal is established based on the Cartesian coordinate system. As shown in Figure 1, the pump light enters the Tm:YAP slab from the two end faces along the x-axis. When the pump laser is transmitted in the laser slab, the pump energy is gradually absorbed by the crystal. Assuming the spatial distribution of the pump light is flat-top, the heat distribution inside the double-end-pumped Tm:YAP crystal can be expressed as:

$$Q(x, y, z) = \alpha\eta \times [\frac{P_1}{S_1}\exp(-\alpha x) + \frac{P_2}{S_2}\exp(-\alpha(L - x))], x \in [0, L] \tag{1}$$

where $Q(x, y, z)$ is the heat per unit volume, α is the absorption coefficient of pump light in Tm:YAP crystal which is mainly dependent on the doping concentration of the Tm^{3+} and the wavelength of the pump light. P_1 and P_2 are the pump power entering the crystal from the left and right end faces, respectively. S_1 and S_2 are the spot sizes of the corresponding pump light. Generally, P_1 equals P_2, and S_1 equals S_2. η is the thermogenesis efficiency which can be calculated by:

$$\eta = 1 - q_e\frac{\lambda_P}{\lambda_L} \tag{2}$$

where q_e is the quantum efficiencies, λ_P and λ_L are the wavelengths of the pump light and the laser, respectively. So, the transient heat conduction equation for an anisotropic Tm:YAP slab crystal can be given by [12]:

$$k_x\frac{\partial^2 T}{\partial x^2} + k_y\frac{\partial^2 T}{\partial y^2} + k_z\frac{\partial^2 T}{\partial z^2} + Q(x, y, z) = \rho c\frac{\partial T}{\partial t} \tag{3}$$

where k_x, k_y, and k_z are the thermal conductivities of the Tm:YAP along the x, y, and z-axis, respectively, ρ is the density and c is the heat capacity. A thin indium layer (no more than 50 µm) is sandwiched between the Tm:YAP cooling surface and the heat sink to ensure good thermal contact. The heat sink is assumed to dissipate the heat quickly enough, which means that the boundary condition of the two big surfaces is:

$$T|_{z=\pm\frac{D}{2}} = T_{.c} \tag{4}$$

where T_c is the temperature of the cooling water, D is the thickness of the Tm:YAP, and the other four surfaces are the air convection heat transfer.
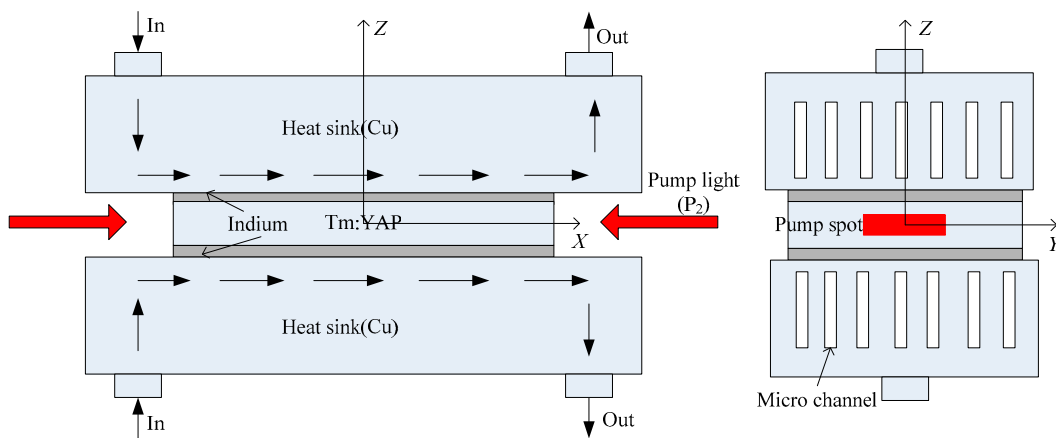

Figure 1. The model of LD-pumped Tm:YAP crystal.

3. Thermal Analysis of the Tm:YAP

The common parameters used in the simulation are shown in Table 1. The a-cut (*x*-axis) Tm:YAP is 4 at.% with the dimension of $1 \times 6 \times 8$ mm 4 at.%. The pump light with flat-top distribution enters the Tm:YAP from the two end faces (1×6) with the power of 100 W and the spots of 0.5×2 mm. The wavelength of the pump light and the laser are 795 nm and 1990 nm, respectively. The quantum efficiency is 1.964, so the thermogenesis efficiency is 0.215 which can be calculated by Equation (2). The absorption coefficient of the a-cut 4 at.% Tm:YAP is 3.75 cm^{-1} which is used in our preliminary work [13].

Table 1. Parameters of Tm:YAP used in the calculations [14–16].

Parameter	Symbol	Value
Thermal conductivity	K, Wm^{-1} K^{-1}	11.6//a, 9.9//b, 12.3//c
Thermal expansion coefficient	α_T, 10^{-6} K^{-1}	9.5//a, 4.3//b, 10.8//c
Poisson ratio	ν	0.3
Thermally-induced refractive index coefficient	dn/dT, 10^{-6} K^{-1}	8.3//a, 7//b, 11.7//c
Density	ρ, Kg/m^3	5350
Thermogenesis efficiency	η	0.215
Young's modulus	E, Gpa	318
Pump Power	$P_1 = P_2$, W	100
Heat capacity	c, JKg^{-1} K^{-1}	419
Absorption coefficient	α, cm^{-1}	3.75 @ 4 at.%
		2.62 @ 3 at.%
		1.9 @1 at.%
Size of Tm:YAP	$D \times W \times L$, mm	$1 \times 6 \times 8$
Size of pump spots,	$d \times w$, mm	0.5×2
Wavelength of pump light	λ_P, nm	795
Wavelength of laser	λ_L, nm	1990
Ambient and cooling water temperature	T_c, K	300

Figure 2 shows the heat power density, temperature, stress, and deformation distribution inside the Tm:YAP with a pump power of 100 W from each end face. According to the absorption coefficient and the size of the Tm:YAP crystal in Table 1, it can be calculated that about 95% of the pump light is absorbed by the crystal, thus, generating 40.85 W heat in the crystal. Along the pump direction, as shown in Figure 2a, the maximum heat power density is 8.5×10^9 W/m^3 which appears on the two end faces of the Tm:YAP crystal. Moreover, the minimum power density appears in the middle of the crystal, with a value of 3.5×10^9 W/m^3. Accordingly, the maximum temperature inside the crystal appears at the center of the pump end face, with a value of 358 K, as shown in Figure 2b. The lowest temperature is at the two main cooling surfaces, with a value of 300 K which is equal to the temperature of the cooling water. The existence of a temperature gradient leads to thermal stress in the crystal. Under the condition that the two large planes are fixed constraints, the stress distribution in the crystal is shown in Figure 2c. The maximum thermal stress occurs at the junction of the pump end face and the large cooling surface with a value of 4.02×10^7 N/m^2. Thermal distortion will cause obvious thermal deformation at the end faces, as shown in Figure 3, and the maximum deformation can reach 5.2×10^{-5} mm.

The thermal effect under different pump power is also calculated when other conditions remain unchanged. Figures 3 and 4 show the distribution of temperature, stress, and thermal deformation when the single-end pump power is 300 W and 500 W. The maximum temperature increases to 474 K and 589 K, respectively, with the single-end pump power of 300 W and 500 W. Accordingly, the maximum thermal stress is 1.05×10^8 N/m^2 and 1.7×10^8 N/m^2. Moreover, the maximum deformation of the end face is 1.3×10^{-4} mm and 2.2×10^{-4} mm.
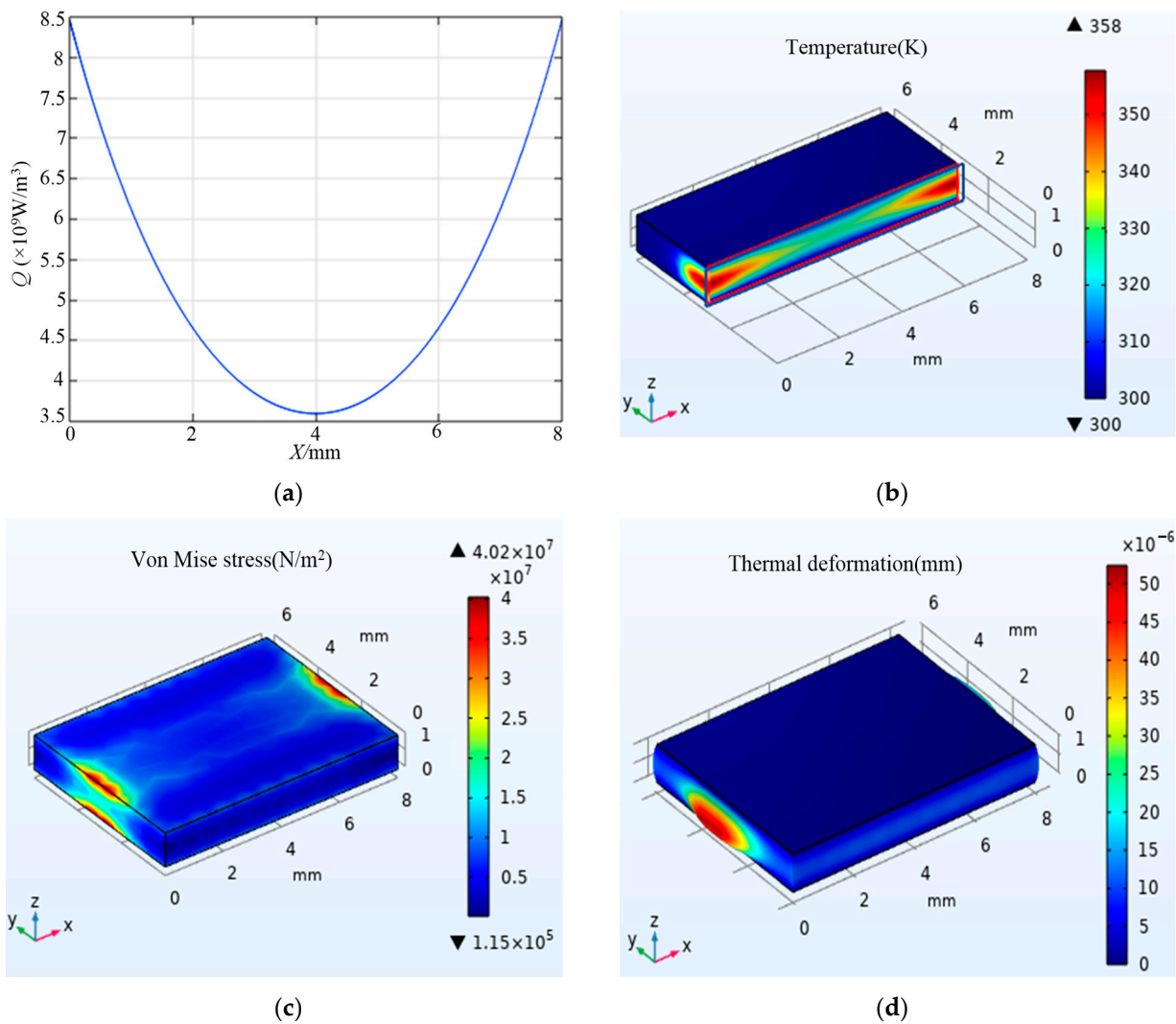
Figure 2. The heat power density (**a**), temperature (**b**), stress (**c**), and thermal deformation (**d**) distribution inside the Tm:YAP with a pump power of 100 W from each end face.
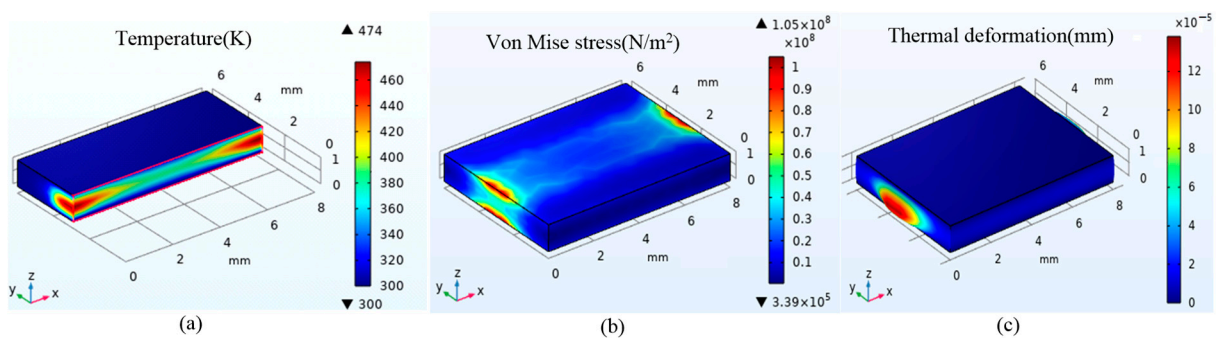

Figure 3. The temperature (**a**), stress (**b**), and thermal deformation (**c**) distribution inside the Tm:YAP with a pump power of 300 W from each end face.
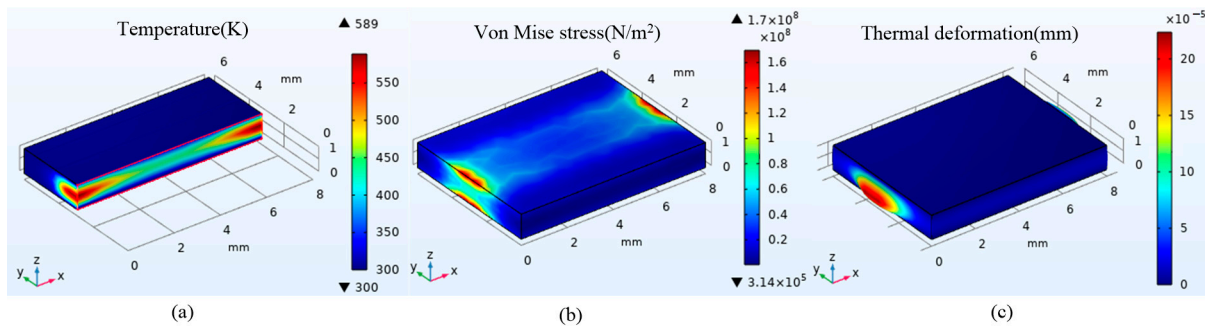
Figure 4. The temperature (**a**), stress (**b**), and thermal deformation (**c**) distribution inside the Tm:YAP with a pump power of 500 W from each end face.

From Figures 2–4, it can be seen that under high-power pumping, the crystal has a large temperature gradient along the direction of the pump light, which is mainly caused by the absorption law of the crystal to pump light. In order to improve the uniformity of pump light absorption in crystals, gradient doping technology is applied to high-power solid-state lasers. The ideal gradient doping allows the pump light to be evenly absorbed by the crystal, which means $dP_{absorbed}/dx = 0$. In practice, perfect gradient doping is difficult to achieve, and a limited number of doping concentrations will be selected in general engineering applications. To improve the internal thermal distribution of the Tm:YAP crystal, the doping concentration of 1 at.%, 3 at.%, and 4 at.% is designed in the Tm:YAP. Moreover, un-doped YAP is added at both ends of the crystal to improve the thermal distortion of the end face, as shown in the Figure 5. The absorption coefficients of Tm:YAP with different doping concentrations are shown in Table 1. In order to ensure that the pump power absorbed in each doping section is basically the same, the lengths of each section are set $L_0 = 3$ mm, $L_1 = L_5 = 2.2$ mm, $L_2 = L_3 = 2.4$ mm, and $L_3 = 2$ mm, respectively. Figure 6 shows the heat power density, temperature, stress, and deformation distribution inside the grad-doping Tm:YAP with a pump power of 100 W from each end face. Compared with Figure 2, the heat distribution with gradient doping is more uniform, with a value between 2.9 and 4.4×10^9 W/m^3. Accordingly, the maximum temperature, stress, and deformation are also reduced to 325 K, 8.45×10^6 N/m^2, and 9.3×10^{-6} mm. When the single-end pump power is increased to 500 W, the thermal effect of Tm:YAP with gradient doping is shown in Figure 7. Compared to Figure 4, the improvement of the thermal effect is more significant as the pump power increases for the gradient doping Tm:YAP.
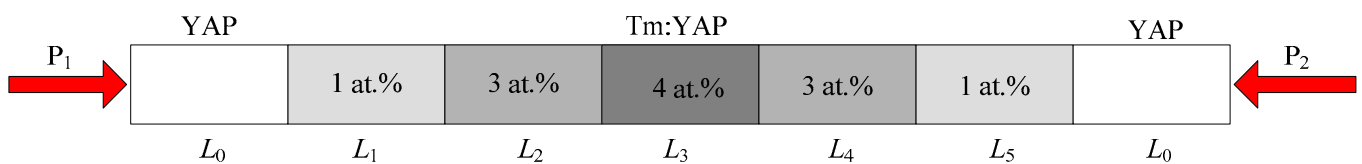

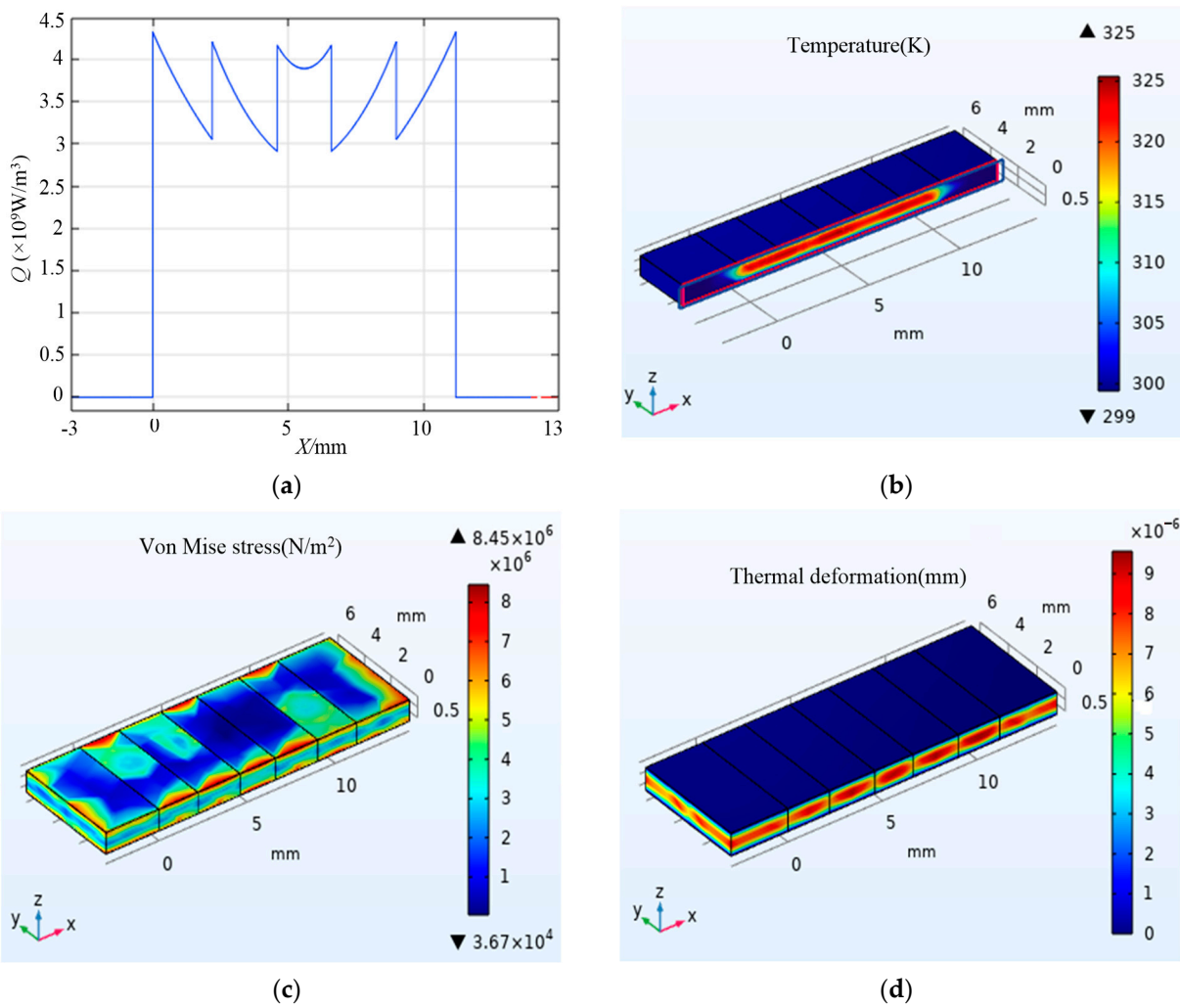**Figure 5.** Schematic diagram of gradient doping Tm:YAP.

Figure 6. The heat power density (**a**), temperature (**b**), stress (**c**), and thermal deformation (**d**) distribution inside the grad-doping Tm:YAP with a pump power of 100 W from each end face.
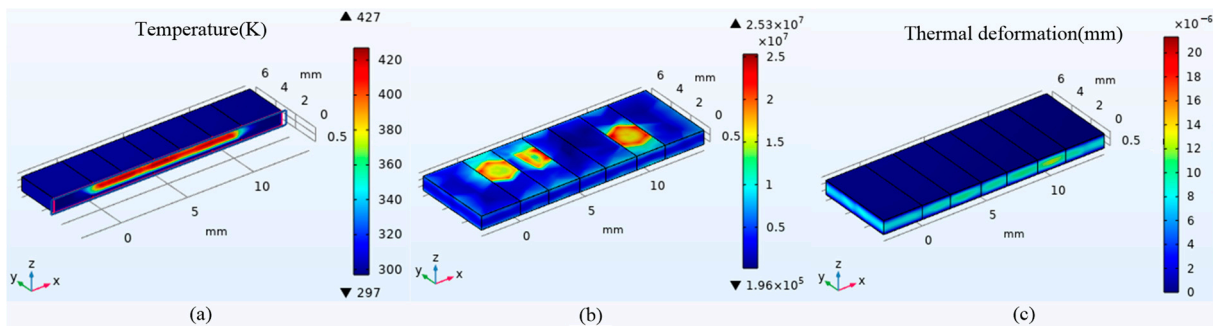

Figure 7. The temperature (**a**), stress (**b**), and thermal deformation (**c**) distribution inside the grad-doping Tm:YAP with a pump power of 500 W from each end face.

In the previous calculation, the boundary condition of the two large faces are set to a constant temperature, which is equal to the cooling temperature. In the actual thin-slab structure, the heat inside the crystal is generally taken away by the heat sink. According to the previous research results [17], a micro-channel heat sink which is made of copper with a thermal conductivity of 401 W/mK is designed as shown in Figure 8. The indium layer between the Tm:YAP to the heat sink is very thin and the heat is transferred very

quickly from the Tm:YAP to the heat sink. Therefore, in the finite element analysis, the indium layer is neglected. The size of h_1 and h_2 are 0.5 mm and 6 mm, respectively. The sum of the channel width (t_1) and rib width (t_2) is 1 mm. The duty cycle (t) is defined by $t = t_1/(t_1 + t_2)$ to optimize the ratio of the channel width and rib width. Forced water convection used in the micro-channel to exchange heat with the convection heat transfer coefficient is 15,000 W/m^2 K. Figure 9a shows the temperature distribution of the Tm:YAP cooled by heat sink with a duty cycle of 0.4. Comparing Figures 2b and 9a, the temperature distribution in the Tm:YAP crystal is similar. The maximum temperature increases by 5 K. In order to obtain a better heat dissipation effect, the micro-channel width is reduced while keeping the duty cycle unchanged. Figure 9b shows the temperature distribution in Tm:YAP with a micro-channel width of 0.2 mm. When the duty cycle is kept constant, the number of micro-channels is doubled, and the temperature distribution is closer to Figure 2b, which indicates that the micro-channel structure has sufficient cooling capacity for high-power thin-slab Tm:YAP crystal.
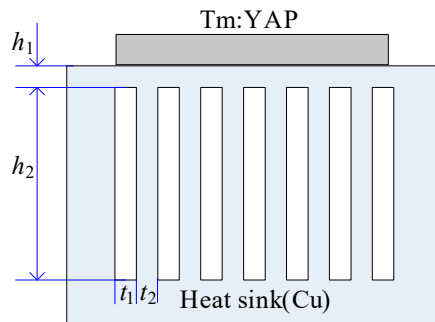

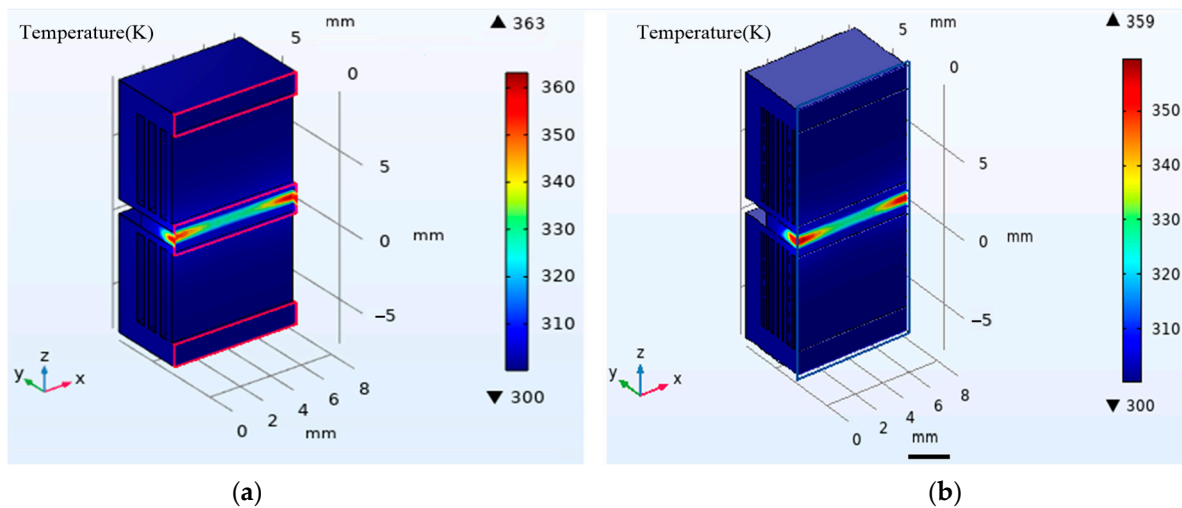**Figure 8.** Cooling heat sink with micro-channel structure.

Figure 9. The temperature distribution inside the Tm:YAP at the duty cycle of 0.4 with a pump power of 100 W from each end face: (**a**) $t_1 = 0.4$, (**b**) $t_1 = 0.2$.

4. Conclusions

This study aimed to investigate the thermal problem in Tm:YAP crystal under high-power pumping and the thermal problem in the crystal was studied in detail by using the finite element method from the perspective of heat generation and removal. The results show that when the total pump power of the crystal is 200 W, 600 W, and 1000 W, the gradient doping technology can effectively improve the thermal distribution in the Tm:YAP crystal. Moreover, the design of the micro-channel structure is also the key to improving the heat dissipation capacity of Tm:YAP crystal. By reasonably optimizing the size of the

micro-channel, the heat elimination capacity of the thin-slice structure Tm:YAP can be effectively improved.

Author Contributions: Methodology, J.S. and X.C.; software, J.S. and Q.L.; validation, J.S. and X.C.; formal analysis, J.S. and X.C.; investigation, J.S. and X.W.; data curation, Q.L and X.W.; writing—original draft preparation, J.S. and Q.L.; writing—review and editing, X.C. and X.W.; supervision, X.C.; funding acquisition, J.S. All authors have read and agreed to the published version of the manuscript.

Institutional Review Board Statement: Not applicable.

Informed Consent Statement: Not applicable.

Data Availability Statement: The data underlying the results presented in this paper are not publicly available at this time but may be obtained from the authors upon reasonable request.

Conflicts of Interest: The authors declare no conflict of interest.

References

1. Henderson, S.W.; Hale, C.P.; Magee, J.R.; Kavaya, M.J.; Huffaker, A.V. Eye-safe coherent laser radar system at 2.1 μm using Tm, Ho: YAG lasers. *Opt. Lett.* **1991**, *16*, 773–775. [CrossRef] [PubMed]
2. Fan, T.Y.; Huber, G.; Byer, R.L.; Mitzscherlich, P. Spectroscopy and diode laser-pumped operation of Tm, Ho: YAG. *IEEE J. Quantum Electron.* **1988**, *24*, 924–933. [CrossRef]
3. Dergachev, A.; Armstrong, D.; Smith, A.; Drake, T.; Dubois, M. 3.4-μm ZGP RISTRA nanosecond optical parametric oscillator pumped by a 2.05-μm Ho: YLF MOPA system. *Opt. Express* **2007**, *15*, 14404–14413. [CrossRef] [PubMed]
4. Elder, I.F.; Payne, M.J.P. Lasing in diode-pumped Tm: YAP, Tm, Ho: YAP and Tm, Ho: YLF. *Opt. Commun.* **1998**, *145*, 329–339. [CrossRef]
5. Coluccelli, N.; Galzerano, G.; Parisi, D.; Tonelli, M.; Laporta, P. Diode-pumped single-frequency Tm: $LiLuF_4$ ring laser. *Opt. Lett.* **2008**, *33*, 1951–1953. [CrossRef] [PubMed]
6. Huang, H.; Hu, H.; Lin, Z.; Deng, J.; Huang, J.; Zheng, H. Anisotropic thermal analyses of a high efficiency Tm: YAP slab laser and its intra-cavity pumping for Ho lasers. *Opt. Express* **2020**, *28*, 20930–20942. [CrossRef] [PubMed]
7. Elder, I.F.; Payne, J. Diode-pumped, room-temperature Tm: YAP laser. *Appl. Opt.* **1997**, *36*, 8606–8610. [CrossRef] [PubMed]
8. Jun, C.; Yu, D. High power double-end-pumped Tm: YAP slab laser. *Electro-Opt. Technol. Appl.* **2017**, *32*, 9–14.
9. Mao, Y.; Gao, Y.; Wang, L. 254 W laser-diode dual-end-pumped Tm: YAP InnoSlab laser. *Appl. Opt.* **2020**, *59*, 8224–8227. [CrossRef] [PubMed]
10. Huang, H.; Ruan, K.; Hu, H.; Deng, J.; Huang, J.; Weng, W.; Lin, W. Above 10 W 2130 nm Ho: YAP laser intra-cavity pumped with composite YAP/Tm: YAP laser. *Opt. Laser Technol.* **2021**, *136*, 106733. [CrossRef]
11. Ligang, Y.; Shouhuan, Z.; Hong, Z.; Guo, C.; Lei, W.; Bao, L.; Keqiang, W. 109.5 W output 1.94 micron Tm: YAP solid-state laser. *Infrared Laser Eng.* **2019**, *48*, 0405006. [CrossRef]
12. Dong, J.Y.; Cui, J.W.; Wen, Y.; Wu, C.T.; Wang, C. High-effective mitigation of thermal effect in multi segment and multi concentration (MSMC) Tm: YAG crystal. *Infrared Phys. Technol.* **2022**, *122*, 104104. [CrossRef]
13. Cheng, X.; Fan, M.; Cao, J.; Shang, J. Research on the thermal effect and laser resonator of diode-pumped thin-slab Tm: YAP lasers. *Optik* **2019**, *176*, 32–37. [CrossRef]
14. Dong, Q.; Zhao, G.; Chen, J.; Ding, Y.; Zhao, C. Growth and anisotropic thermal properties of biaxial Ho: $YAlO_3$ crystal. *J. Appl. Phys.* **2010**, *108*, 023108. [CrossRef]
15. Aggarwal, R.L.; Ripin, D.J.; Ochoa, J.R.; Fan, T.Y. Measurement of thermo-optic properties of $Y_3Al_5O_{12}$, $Lu_3Al_5O_{12}$, $YAlO_3$, $LiYF_4$, $LiLuF_4$, BaY_2F_8, $KGd(WO_4)_2$, and $KY(WO_4)_2$ laser crystals in the 80–300 K temperature range. *J. Appl. Phys.* **2005**, *98*, 103514. [CrossRef]
16. Zhan, X.; Li, Z.; Liu, B.; Wang, J.; Zhou, Y.; Hu, Z. Theoretical prediction of elastic stiffness and minimum lattice thermal conductivity of $Y_3Al_5O_{12}$, $YAlO_3$ and $Y_4Al_2O_9$. *J. Am. Ceram. Soc.* **2012**, *95*, 1429–1434. [CrossRef]
17. Cheng, X.; Shang, J. Thermal behavior of micro-channel cooled thin-slab Fe: ZnSe lasers. *Optik* **2017**, *143*, 66–70. [CrossRef]